AD-A188 799 COHERENT LASER RADAR SYSTEM THEORY(U) MASSACHUSETTS 1/1
INST OF TECH CAMBRIDGE RESEARCH LAB OF ELECTRONICS
J H SHAPIRO 05 NOV 87 ARO-21192.6-PH DAAG29-84-K-0095
UNCLASSIFIED F/G 17/9 NL

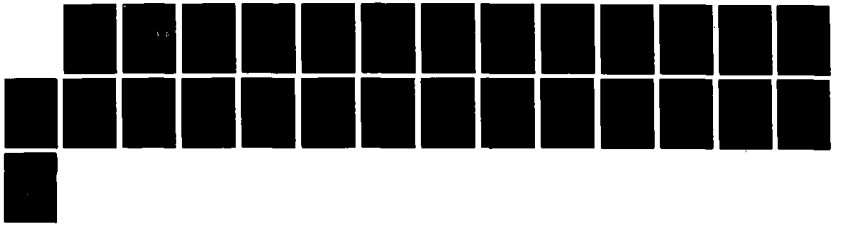


1.25
1.4
1.6
1.1
1.0

ARO 21192.6-PH

(2)

COHERENT LASER RADAR SYSTEM THEORY

Final Report

Jeffrey H. Shapiro
Massachusetts Institute of Technology

U.S. Army Research Office Contract DAAG29-84-K-0095

Period Covered: 8/1/84 – 9/30/87

Report Date: 11/5/87

UNCLASSIFIED

SECURITY CLASSIFICATION OF THIS PAGE

AD-A188 759

REPORT DOCUMENTATION PAGE

1a. REPORT SECURITY CLASSIFICATION: Unclassified	1b. RESTRICTIVE MARKINGS
2a. SECURITY CLASSIFICATION AUTHORITY	3. DISTRIBUTION/AVAILABILITY OF REPORT: Approved for public release; distribution unlimited
2b. DECLASSIFICATION/DOWNGRADING SCHEDULE	
4. PERFORMING ORGANIZATION REPORT NUMBER(S)	5. MONITORING ORGANIZATION REPORT NUMBER(S): ARO 21192.6-PH
6a. NAME OF PERFORMING ORGANIZATION: Research Laboratory of Electronics, Massachusetts Institute of Technology; 6b. OFFICE SYMBOL (If applicable)	7a. NAME OF MONITORING ORGANIZATION
6c. ADDRESS (City, State and ZIP Code): 77 Massachusetts Avenue, Cambridge, MA 02139	7b. ADDRESS (City, State and ZIP Code)
8a. NAME OF FUNDING/SPONSORING ORGANIZATION: U.S. Army Research Center; 8b. OFFICE SYMBOL (If applicable)	9. PROCUREMENT INSTRUMENT IDENTIFICATION NUMBER: DAAG 29-84-K-0095
8c. ADDRESS (City, State and ZIP Code): P. O. Box 12211, Research Triangle Park, North Carolina 27709	10. SOURCE OF FUNDING NOS. — PROGRAM ELEMENT NO.; PROJECT NO.: P-21192-PH; TASK NO.; WORK UNIT NO.
11. TITLE (Include Security Classification): Coherent Laser Radar System Theory	
12. PERSONAL AUTHOR(S): J. H. Shapiro	
13a. TYPE OF REPORT: Final Report; 13b. TIME COVERED: FROM 8/1/84 TO 9/30/87; 14. DATE OF REPORT (Yr., Mo., Day): 5 November 1987; 15. PAGE COUNT: 26	
16. SUPPLEMENTARY NOTATION	
17. COSATI CODES — FIELD; GROUP; SUB. GR.	18. SUBJECT TERMS (Continue on reverse if necessary and identify by block number): Laser radar theory, Laser speckle, Radar system theory

19. ABSTRACT (Continue on reverse if necessary and identify by block number)

This program is aimed at developing a system theory for the emerging technology of multifunction coherent CO_2 laser radars. It builds upon previous work funded by U.S. Army Research Office Contract DAAG29-80-K-0022

20. DISTRIBUTION/AVAILABILITY OF ABSTRACT: UNCLASSIFIED/UNLIMITED ☒ SAME AS RPT. ☐ OTIC USERS ☐	21. ABSTRACT SECURITY CLASSIFICATION: Unclassified
22a. NAME OF RESPONSIBLE INDIVIDUAL: Kyra M. Hall, RLE Contract Reports	22b. TELEPHONE NUMBER (Include Area Code): (617) 253-2569; 22c. OFFICE SYMBOL

DD FORM 1473, 83 APR EDITION OF 1 JAN 73 IS OBSOLETE.

UNCLASSIFIED

SECURITY CLASSIFICATION OF THIS PAGE

Table of Contents

COHERENT LASER RADAR SYSTEM THEORY

Abstract

Coherent laser radars for tactical sensor applications are under development at a number of laboratories, based on the mid-infrared technology of CO_2 lasers and HgCdTe photodetectors. Under U.S. Army Research Office Contract DAAG29-84-K-0095, a program of research was pursued to advance the system theory of such radars, and to corroborate these advances through experiments performed using the test bed coherent laser radars of the MIT Lincoln Laboratory Opto-Radar Systems Group. Toward those ends, fundamental results were derived for the transverse and longitudinal correlation scales of speckle targets observed via heterodyne detection, and pixel-level statistics were derived and experimentally verified for 2-D pulsed imager radars that use peak-detection pre-processors. In addition, a multipixel multidimensional target detection theory was established whose quasi-optimal processors coincide with some ad-hoc designs already in use, and whose performance analysis provides unprecedented insights into the tradeoffs between radar system parameters and target-detection capability. Work was also begun on the theory of unconventional laser radar imagers, e.g., synthetic aperture systems, and on target-tracking theory for extended speckle objects.

I. Research Summary

The development of laser technology offers new alternatives for the problems of target detection and imaging. Indeed, coherent laser radars based on the mid-infrared technology of CO_2 lasers and HgCdTe photodetectors are under development at a number of laboratories [1] - [5]. The performance of such systems is strongly affected by the speckle patterns that are produced by target roughness on wavelength scales [6], [7]. This document is the final report on a research program to develop a quantitative system theory for such radars through a combination of analysis and experiment. The central issues for this program were the impact of laser speckle on fundamental pixel statistics [8] - [10] and on the design and performance of multipixel target detection processors [11] - [13]. In both cases, emphasis was placed on multidimensional, e.g., range and intensity, measurements. Moreover, the fundamental pixel statistics, which served as the foundation for the detection analysis, were experimentally verified [9], [10] under a collaboration arrangement with the Opto-Radar Systems Group of the MIT Lincoln Laboratory using one of their test bed CO_2 laser radars [1]. Finally, preliminary analyses were begun in the areas of unconventional laser radar imaging [14] and laser radar tracking theory [15], and laser reflectometer measurements [16] were used to support theory from [17]. In what follows, we shall summarize the principal results that were obtained in the preceding problem areas.

Speckle Statistics [8]:

In order to understand the impact of speckle fluctuations on the full panoply of coherent laser radar measurements, we derived the transverse and longitudinal degrees of coherence for speckle targets observed via heterodyne detection. This work elucidated hitherto unidentified interactions between

various measurement-configuration parameters that affect speckle-target correlation scales, and hence laser radar performance.

Peak-Detection Pixel Statistics [9], [10]:

In 2-D pulsed imager and 2-D Doppler imager radars, the intermediate frequency return signals are generally filtered, envelope detected, thresholded, and peak detected in a pre-processor subsystem [1], [18]. We have analyzed and experimentally verified the resulting pixel statistics produced with such systems by speckle targets, and have quantified the associated dropout and anomaly effects in range and Doppler measurements.

Multipixel Multidimensional Detection Theory [11] - [13]:

We have addressed the somewhat idealized problem in which a 2-D pulsed imager laser radar is used to detect the presence of an extended statistically-uniform speckle target embedded in a statistically-uniform extended speckle background when the target location and target contrast are unknown. Quasi-optimum intensity-only, range-only, and joint range-intensity processors were derived, and receiver operating characteristics were computed for the intensity-only and range-only cases. This work is important because it builds from the correct pixel statistics found in [9], [10], and because the intensity-only and range-only processors coincide with ad hoc approaches already in use. The work's greatest significance, however, lies in its quantitative performance predictions, which permit assessing tradeoffs between radar system parameters, e.g., spatial resolution, range resolution, etc., and target detection performance.

Target Reflectivity Measurements [16]:

We performed a series of reflectivity measurements on a variety of calibration plates and spheres using an incoherent 10.6 μm wavelength reflec-

tometer. Reflectometer data for the plates were found to be in close agreement with measurements collected with the MIT Lincoln Laboratory 2-D pulsed imager laser radar test bed, as expected from theory [17].

Unconventional Laser Radar Imaging [14]:

We have been developing system theory results for laser radar versions of 1-D and 2-D synthetic aperture radars (SARs) and range-Doppler (RD) imagers. In both cases our focus has been to understand the combined effects of target speckle and local-oscillator shot noise on system performance. The effects of atmospheric turbulence and laser frequency instability are also being treated.

Laser Radar Tracking Theory [15]:

We have begun developing a theory for laser radar tracking of extended speckle targets. Thus far, we have solved the track-while-image problem in which an intensity centroid estimate from the nth image frame is used as the observation equation for a Kalman-filter tracker. The updated target position estimate obtained from this tracker is then used to set the radar's optical axis for the $(n+1)$st image frame.

II. References

[1] R.J. Hull and R.C. Harney, "Compact Infrared Radar," Proc. SPIE 227, 162 (1980).

[2] M.J. Post, R.A. Richter, R.M. Hardesty, T.R. Lawrence, and F.F. Hall, Jr., "National Oceanic and Atmospheric Administration's (NOAA) Pulsed, Coherent, Infrared Doppler Lidar - Characteristics and Data," Proc. SPIE 300, 60 (1981).

[3] I. Renhorn, O. Steinvall, D. Letalick, K. Gullberg, T. Claesson, and A. Widén, "Performance Study of a Coherent Laser Radar," Proc. SPIE 415, 39 (1983).

[4] R. Foord, R. Jones, J.M. Vaughan, and D.V. Willetts, "Precise Comparison of Experimental and Theoretical SNRs in CO_2 Laser Heterodyne Systems," Appl. Opt. 22, 3787 (1983).

[5] J.Y. Wang, B.J. Bartholomew, M.L. Streiff, and E.F. Starr, "Imaging CO_2 Laser Radar Field Tests," Appl. Opt. 23, 2565 (1984).

[6] J.W. Goodman, "Some Effects of Target-Induced Scintillation on Optical Radar Performance," Proc. IEEE 53, 1688 (1965).

[7] J.H. Shapiro, B.A. Capron, and R.C. Harney, "Imaging and Target Detection with a Heterodyne-Reception Optical Radar," Appl. Opt. 20, 3292 (1981).

[8] J.H. Shapiro, "The Correlation Scales of Laser Speckle in Heterodyne Detection," Appl. Opt. 24, 1883 (1985).

[9] R.W. Reinhold, "Reflectivity Determination Using a Peak Detecting Coherent Laser Radar," S.M. thesis, Dept. of Elect. Engr. and Comput. Sci., MIT, June 1985.

[10] J.H. Shapiro, R.W. Reinhold, and D. Park, "Performance Analyses for Peak-Detecting Laser Radars," Proc. SPIE 663, 38 (1986).

[11] M.B. Mark, "Multipixel, Multidimensional Laser Radar System Performance," Ph.D. thesis, Dept. of Elect. Engr. and Comput. Sci., MIT, Aug. 1986.

[12] M.B. Mark and J.H. Shapiro, "Multipixel, Multidimensional Laser Radar System Performance," Proc. SPIE 783 (in press; preprint attached as Appendix).

[13] S.M. Hannon, "Performance Analysis of Quasi-Optimal, Multipixel Laser Radar System Processors," S.M. thesis, Dept. of Elect. Engr. and Comput. Sci., MIT, June 1987.

[14] D. Park, "Unconventional Laser Radars," Ph.D. thesis proposal, Dept. of Elect. Engr. and Comput. Sci., MIT, October 1986.

[15] R.H. Enders, "Laser Radar Tracking Theory: Track-While-Image Operation," unpublished Ph.D. thesis research, Dept. of Elect. Engr. and Comput. Sci., MIT, 1987.

[16] E.A. Rappaport, "CO_2 Laser Reflectometer Measurements," S.B. thesis, Dept. of Electr. Engr. and Comput. Sci., MIT, June 1987.

[17] J.H. Shapiro, "Target-Reflectivity Theory for Coherent Laser Radars," Appl. Opt. 21, 3398 (1982).

[18] A.B. Gschwendtner, R.C. Harney, and R.J. Hull, "Coherent IR Radar Technology," in D.K. Killinger and A. Mooradian, eds., Optical and Laser Remote Sensing (Springer-Verlag, Berlin, 1983).

III. Personnel

The research reported here was carried out by

Prof. Jeffrey H. Shapiro, principal investigator

Dr. Robert J. Hull, senior investigator

Capt. Martin B. Mark, graduate student (Ph.D. 1986)

Mr. Hai V. Tran, research assistant (S.M. 1985)

Mr. Robert W. Reinhold, research assistant (S.M. 1985)

Mr. Stephen M. Hannon, research assistant (S.M. 1987)

Mr. Dongwook Park, research assistant

Mr. Robert H. Enders, research assistant

Mr. Donald E. Bossi, research assistant

Mr. Ethan A. Rappaport, undergraduate student (S.B. 1987)

IV. Publications

The following journal articles, meeting papers, and theses have been produced under U.S. Army Research Office Contract DAAG29-84-K-0095.

1. J.H. Shapiro, "Precise Comparison of Experimental and Theoretical SNRs in CO_2 Laser Heterodyne Systems: Comments," Appl. Opt. 24, 1245-1247 (1985).
2. J.H. Shapiro, "Correlation Scales of Laser Speckle in Heterodyne Detection," Appl. Opt. 24, 1883-1888 (1985).
3. J.H. Shapiro, "Laser Radar System Theory," in Digest of Topical Meeting on Optical Remote Sensing of the Atmosphere (Opt. Soc. Am., Washington, D.C., 1985).
4. J.H. Shapiro, "The Correlation Scales of Laser Speckle in Heterodyne Detection," in Proceedings of the 3rd Topical Meeting on Coherent Laser Radar: Technology and Applications (Coherent Laser Radar Meeting, Malvern, 1985).
5. H.V. Tran, "Speckle Target Returns Observed with a Doppler Radar: A Simulation Approach," S.M. Thesis, Dept. of Elect. Engr. and Comput. Sci., MIT, Jan. 1985.
6. R.W. Reinhold, "Reflectivity Determination Using a Peak Detecting Coherent Laser Radar," S.M. Thesis, Dept. of Elect. Engr. and Comput. Sci., MIT, June 1985.
7. M.B. Mark, "Multipixel Multidimensional Laser Radar System Performance," Ph.D. Thesis, Dept. of Elect. Engr. and Comput. Sci., MIT, Aug. 1986.
8. J.H. Shapiro, R.W. Reinhold, and D. Park, "Performance Analyses for Peak-Detecting Laser Radars," Proc. SPIE 663, 38-56 (1986).
9. S.M. Hannon, "Analysis of Quasi-Optimal Multipixel Laser Radar System Processors," S.M. Thesis, Dept. of Electr. Engr. and Comput. Sci., MIT, June 1987.

10. E.A. Rappaport, "CO_2 Laser Reflectometer Measurements," S.B. Thesis, Dept. of Elect. Engr. and Comput. Sci., MIT, June 1987.

11. M.B. Mark and J.H. Shapiro, "Multipixel Multidimensional Laser Radar System Performance," Proc. SPIE 783 (in press, preprint attached as Appendix).

APPENDIX

Multipixel, multidimensional laser radar system performance

Martin B. Mark

Department of Electrical Engineering
United States Air Force Academy, Colorado 80840

Jeffrey H. Shapiro

Department of Electrical Engineering and Computer Science
Massachusetts Institute of Technology, Cambridge, Massachusetts 02139

Abstract

The superb angular, range, and Doppler resolutions of coherent laser radars have led developers to design imaging radars in multiple measurement dimensions. Designing processors to detect targets in the images generally proceeds in an ad hoc fashion and it is difficult to predict the performance of the resulting processors. This paper proposes simplified statistical models for the target, radar, and signals then uses classical detection theory to derive quasi-optimal processors which take advantage of the multipixel, multidimensional nature of the image. The target model is of a radar looking down at a vertical target against a uniform, sloping background. The paper also presents the receiver operating characteristics (ROCs) for the resulting generalized likelihood ratio test (GLRT) processors. The receivers may use any combination of intensity, range, and Doppler measurements. The target reflectivity, range, and angular location are unknown and the background reflectivity is also unknown. The forms of the quasi-optimal receivers provide analytical confirmation of the principles used in many ad hoc processors. The ROCs not only give bounds on the performance of any ad hoc processors and prove the range-only processors are usually superior to the intensity-only processors, but go on to predict how much better and under what conditions. The ROCs also predict how performance changes as a function of resolution in one or several measurement dimensions.

Introduction

The advent of laser sources with high stability, spectral purity, and sufficient power has allowed system designers to translate much of microwave radar theory to the optical regime.[1,2,3] Because the spatial resolution obtainable at optical and infrared (IR) wavelengths is on the order of microradians, most researchers have opted for building and analyzing systems which perform a raster scan of the target and build an image of the target much like a television image. These radars are capable of building intensity, range, or Doppler images or using any combination of these measurement dimensions.[4,5] Although there has been much work on analyzing the statistics of the target returns on a single pixel basis,[6,7,8,9] most of the work on processing the multipixel images has rested on ad hoc processors or parallel results from applications in the fields of robotics, machine vision, and artificial intelligence.[10,11] Although these approaches to image processing have produced useful processors, they ignore the underlying statistical nature of the image and it is very difficult to predict the processor's performance or how the performance might change as various system parameters change. This work extends models and single pixel probability density functions (pdfs) introduced in earlier studies[12] to construct pdfs for the multipixel, multidimensional image data. These density functions (and the results which follow) are suitable for radars which measure target and background reflected intensity, range, velocity (Doppler shift), or any combination of these parameters.[13] (This paper, however, deals only with intensity and range.) The models are slightly simplified, but still allow for unknown target angular location, range, and reflectivity and unknown background reflectivity. Generalized likelihood ratio test (GLRT) processors and their performance measures, including receiver operating characteristics (ROCs), are derived for the binary hypothesis testing problem. From the ROCs it is possible to predict the impact on system performance from changing the various system parameters like radar optics aperture, radar power, range resolution, and Doppler resolution, to name only a few. These ROCs define the fundamental limits to the performance of any processor imposed by the statistics of the signals. They are particularly useful as benchmarks for comparing real processors. The GLRT processors provide analytical confirmation of some of the processing principles used in many ad hoc approaches.

Target and radar models

Binary hypothesis testing

This work is concerned with the problem of deciding whether or not there is a target in a given volume of space. This is the binary hypothesis testing problem[16]: the radar makes measurements (receives target returns) over a volume of space and uses the measurements to decide whether there is a target in the volume (hypothesis H_1 is true) or there is no target in the volume (hypothesis H_0 is true). Figure 1 pictures the problem for a volume defined by the angular uncertainty Ω_u and range uncertainty L_u. The radar makes measurements in the volume by raster scanning the radar beam pattern across the target region defined by the angular uncertainty Ω_u. The radar must discriminate between target and background while it does not know the target's range, angular location, or reflectivity.

IF signal model

The laser radar model will be of a compact, monostatic, coherent laser radar. The radar beam pattern is raster scanned across an uncertainty region Ω_u which may contain a target. The laser transmits a series of pulses so the received signal, after heterodyning, is a series of either target or background returns (depending on which is illuminated) plus local oscillator (LO) shot noise. Each target or background return forms one picture element (pixel) of the resulting raster scanned image. We assume pixels are essentially non-overlapping and, hence, independent. We will consider only purely speckle reflectors in this work. For a ranging radar, the pulses will be assumed to be short duration, transform limited waveforms which do not resolve any range variations within a pixel. We follow the heterodyne detector with a filter whose impulse response is matched to the transmitted waveform. The next step is to square and peak detect the filter output. The peak detector outputs are then two random variables, $\hat{I}$, the intensity of the peak, and $\hat{L}$, the maximum likelihood (ML) estimate of the reflector range. These outputs are our measured data and their pdfs are known. This pre-processor structure is shown in Figure 2. This structure follows that used in many systems currently under study,[15] so the results are easily compared with data from real systems.

Geometry model

Figure 3 shows the model for the laser and target geometry. The radar is above and looking down on the target which is vertical to the ground. The target angular subtense is greater than a radar beam width, so the target is resolved in angle space. We will call M the number of pixels on the target. All target pixels will occur at about the same range since the target is vertical, however, the background pixels will appear to slope away from the radar. Further, if we know the radar's height above the ground and its pointing angle, we can calculate the range to the background if it is reasonably smooth. Our model will assume this range is known. This model is particularly well suited for an airborne radar looking for targets on the ground.

If we know the target size (angular extent) and shape, we can tile the radar field of regard with M target shapes as in Figure 4. We will call one observation of the radar field of regard (MN pixels) a frame and each target shape (M pixels) a subframe. We will henceforth assume the targets align with the subframe boundaries (the subframe contains either an entire target or no part of a target) so the subframes are independent (have no pixels in common). Later research has relaxed this assumption.[16]

Single pixel density functions

In order to derive the optimal processors, we need to know the density functions for the measurements. Since the pixels are all independent, we need to find the density function for a single pixel. From this density we can generate multipixel density functions easily.[12] The single pixel density functions for this receiver structure have been published before and are repeated below. Understanding the density and the resulting processors, however, relies on understanding the operation of the peak detector as well.

We can model the operation of the peak detector by dividing the range uncertainty L_u into Q bins of width equal to the radar range resolution. The output of the square law envelope detector is approximately constant over a bin time and the bins are approximately independent. For any one bin, the intensity output is an exponential random variable with mean 1 if there is no reflector at that range or mean CNR+1 if there is a reflector at that range (where CNR is the usual speckle target radar carrier-to-noise ratio for the reflector[17]). Figure 5 shows the range bin model with the Q bins separated into Q_n bins known to contain the background pixels and Q_m potential target range bins. The target falls in bin Q_t and the background falls in bin Q_b. The peak detector selects the largest of the Q intensity random variables and declares this as the reflector intensity and the

associated range value as the reflector range for the pixel in question. If this procedure selects the wrong bin, we say an anomaly has occurred as pictured in Figure 5.

The resulting marginal statistics are[12]:

$$p_I(x) = (1-e^{-ax})\ (Q-1)\ (1-e^{-x})^{Q-2}\ e^{-x}\ u(x) \ + \ ae^{-x}\ (1-e^{-x})^{Q-1}\ u(x) \tag{1}$$

$$Pr(\hat{Q}=q) = (1-P_A)\ \delta_{qQ_i} + \frac{P_A}{Q-1}\ (1-\delta_{qQ_i}) \tag{2}$$

where $a = (CNR+1)^{-1}$, random variable $\hat{Q}$ is the bin where the peak occurred, Q_i is the bin actually containing the target or background reflector (where i = t or b), and P_A is the probability of an anomaly given by:

$$P_A = a\ \frac{\Gamma(Q)\ \Gamma(a)}{\Gamma(Q+a)} \approx a[\ \log(Q) - 1/2Q + 0.577\ ] \tag{3}$$

where $\Gamma()$ is the gamma function. The approximation is valid for large CNR values.[14]

These results are specifically for the ranging radar. However, it is possible to show an exact duality between all the ranging radar results and those for a Doppler radar.[13] It is also possible to demonstrate an exact duality with a range and Doppler radar if it has an ambiguity function which is unimodal.[13] Henceforth, all results are for the ranging radar with the appropriate analogies to Doppler systems understood.

Binary detection receivers

With pixel statistics in hand, we can derive the optimal receiver for choosing between the two hypotheses H_0 and H_1. We will use the Neyman-Pearson criterion which constrains P_F, the probability of false alarm, to be less than or equal to a specified value and minimizes P_M, the probability of miss.[14] The result is a likelihood ratio test[14]:

$$\Lambda^{(f)}(\bar{r}) = \frac{p_{\bar{R}|H_1}(\bar{r}|H_1)}{p_{\bar{R}|H_0}(\bar{r}|H_0)} \underset{H_0}{\overset{H_1}{\gtrless}} \lambda \tag{4}$$

where the superscript (f) emphasizes the data vector $\bar{r}$ and the likelihood ratio $\Lambda^{(f)}()$ are the measurement data and the likelihood function for the entire frame. Since all pixels give independent measurements (minimal beam overlap) and the target is entirely in one subframe, the frame density function is simply the product of the subframe density functions which are, in turn, the product of the pixel density functions. The threshold λ is chosen to meet the P_F constraint with equality.

Unknown parameters

The density functions introduced in the last section depend on unknown, non-random parameters like the target or background range bin, Q_i. We eliminate the unknown parameters by using the generalized likelihood ratio test (GLRT):[14]

$$\Lambda_g^{(f)}(\bar{r}) = \frac{\max_{\bar{A}}\{p_{\bar{R}|H_1,\bar{A}}(\bar{r}|H_1,\bar{A})\}}{\max_{\bar{A}}\{p_{\bar{R}|H_0,\bar{A}}(\bar{r}|H_0,\bar{A})\}} \underset{H_0}{\overset{H_1}{\gtrless}} \lambda \tag{5}$$

where $\bar{A}$ is the unknown parameter vector. For our problems, the unknown parameters are m_o, the actual subframe containing the target; Q_t, the actual target range bin number; and both target and background CNRs: CNR_T and CNR_B, respectively.

Introducing the GLRT here is a crucial step in the development. The unknown parameters involve the multipixel nature of the target and allow us to extend single pixel statistical analyses to the multipixel case.

We can make additional simplifications to the frame likelihood ratio. Since subframes do not overlap and the target is always aligned with a subframe (by assumption) we can separate the frame density function into subframe density functions which only differ, under hypotheses H_0 and H_1, for the one subframe m_o. We can further simplify the density functions because the unknown parameter vector $\bar{A}$ contains some elements which affect the density under hypothesis H_0 but not under H_1 and vice versa. This fact allows us to make a

simplification for large values of M (the number of subframes per frame). The result is:

$$\Lambda_g^{(f)} = \max_{1\le m\le M} \{\Lambda_{gm}^{(s)}\} \tag{6}$$

$$\Lambda_{gm}^{(s)} = \frac{p_{\bar{R}_m^{(s)}|H_1^{(s)},\hat{A}_1}(\bar{r}_m^{(s)}|H_1^{(s)},\hat{\bar{A}}_I)}{p_{\bar{R}_m^{(s)}|H_0^{(s)},\hat{A}_0}(\bar{r}_m^{(s)}|H_0^{(s)},\hat{A}_0)} \tag{7}$$

where the (s) superscript indicates a subframe quantity and the m subscript is still a subframe index. (Hypothesis $H_1^{(s)}$ indicates a target present in this subframe and hypothesis $H_0^{(s)}$ indicates no target in this subframe). The vectors $\bar{A}_0$ and $\bar{A}_1$ are the portions of the parameter vector $\bar{A}$ affecting the density under hypotheses H_0 and H_1, respectively. The $\hat{}$ indicates an ML estimate of the parameter subvector.

Because of the form of Equation (6) it is easy to show the frame level statistics $P_F^{(f)}$ and $P_M^{(f)}$ depend on the subframe statistics $P_F^{(s)}$ and $P_M^{(s)}$ in a simple fashion:

$$\begin{aligned} P_F^{(f)} &= Pr(\Lambda_g^{(f)} > \lambda \mid H_0) \\ &= 1 - [1 - P_F^{(s)}]^M \\ &\approx M P_F^{(s)} = M\, Pr(\Lambda_{gm}^{(s)} > \lambda \mid H_0^{(s)}) \end{aligned} \tag{8}$$

$$\begin{aligned} P_M^{(f)} &= Pr(\Lambda_g^{(f)} < \lambda \mid H_1) \\ &= P_M^{(s)} [1 - P_F^{(f)}]^{(M-1)/M} \\ &\approx P_M^{(s)} = Pr(\Lambda_{gm}^{(s)} < \lambda \mid H_1^{(s)}) \end{aligned} \tag{9}$$

where the approximations are valid for the usual $P_F^{(s)} \ll 1$ case.

These equations have important physical interpretations. The false alarm probability rises linearly as the number of subframes (the angular search area) increases. The miss probability is approximately independent of the search area. A detection occurs if any subframe statistic clears the threshold, even if it is not the correct subframe. The probability of detection on the wrong subframe is quite small, however, since this is basically a subframe false alarm with probability $P_F^{(s)}$.

Intensity-only processors

First consider the processor which uses only the measured, peak detected intensity for each pixel. Because of the peak detector the pdf for $\hat{I}$ is complicated and it is difficult to derive an exact optimal processor. To derive the processor, we used a Central Limit Theorem approximation to the density. This gives an eminently reasonable processor as we shall shortly see. To analyze the processor performance, there are better approximations to the tails of the density function (based on modified Chernoff bounds)[14] which give more accurate results than the Central Limit Theorem.

Applying the Central Limit Theorem approximation, performing the required algebra, and simplifying the expression,[13] the final log likelihood ratio for the quasi-optimal intensity-only processor is:

$$\begin{aligned} \log \Lambda_g^{(f)} &= \max_{1\le m\le M} \{\log \Lambda_{gm}^{(s)}\} \\ &= \max_{1\le m\le M} \{|\sum_{n=1}^{N} \hat{I}_{mn} - N\hat{\mu}_b|\} \end{aligned} \tag{10}$$

where $\hat{I}_{mn}$ is the measured intensity for the n-th pixel in the m-th subframe, and $\hat{\mu}_b$ is the ML estimate of the background mean intensity under hypothesis H_0:

$$\hat{\mu}_b = \bar{\mu}_b = \frac{1}{MN} \sum_{m=1}^{M} \sum_{n=1}^{N} \hat{I}_{mn} \tag{11}$$

The processor in Equation (10) has a reassuring form. It says we make an estimate of the average background intensity and compare it to the average intensity of each subframe. The subframe whose intensity is most different from the background is declared the target subframe if the difference is greater than the threshold. If the difference is less than the threshold, we declare H_0: no target present. In other words, the processor searches for target-to-background intensity contrast. This is exactly what intuition tells us to do and what many researchers have done with their ad hoc processors.

Range-only processor

Now consider a processor which uses only the range bin information, q_{mn}, the measured bin number where the peak intensity occurred. For this processor we use the single pixel range statistics given earlier, introduce the multipixel statistics by using pixel independence, and make GLRT processors by separating the unknown parameters under hypotheses H_0 and H_1. The approximate generalized likelihood ratio which results is:

$$\Lambda_g^{(f)} = \max_{1 \le m \le M} \{ \Lambda_{gm}^{(s)} \} = \max_{1 \le m \le M} \{ j_m - k_m \} \tag{12}$$

$$\text{where:} \quad j_m = \max_{1 \le Q_{tm} \le Q_T} \{ \sum_{n=1}^{N} \delta_{q_{mn} \hat{Q}_{tm}} \} \quad \text{and} \quad k_m = \sum_{n=1}^{N} \delta_{q_{mn} Q_{bmn}} \tag{13}$$

Here Q_{bmn} is the (known) range bin number for the background in pixel m, n; q_{mn} is the peak detector output bin number for pixel m, n; and $\hat{Q}_{tm}$ is the presumed target range bin number for the m-th subframe. In words, k_m is the number of times the peak detector found the peak intensity occurred at the correct background range in the m-th subframe. Random variable j_m is the number of times the peak detector found the intensity peak at the presumed target range bin in the m-th subframe. The presumed target range bin, for a particular subframe, is the potential target range bin which the peak detector chooses more often than any other potential target range bin for that subframe.

Physically, Equation (12) says the processor determines whether the presumed target range bin or the known background range bin was selected more often by the peak detector for each subframe. The more often the presumed target bin is selected, relative to the background bins, the larger the statistic $\Lambda_{gm}^{(s)}$. If the maximum of these statistics over all M subframes exceeds the threshold, the processor declares H_1: target present. In other words, the processor looks for the range measurements to aggregate or clump in either the known background range bins (if no target is present) or one of the Q_T potential target range bins (if a target is present). Colloquially put, the processor searches for range contrast. In particular, owing to the nature of the Figure 3 geometry, this range contrast can also be called verticality.

Receiver performance results

It is possible, at least in theory, to find performance measures for the processors just derived by integrating the pdfs over the proper ranges, set by the detection threshold, to get P_F and P_M values.[14] In practice it is difficult or impossible to carry out these integrations except numerically or with approximation techniques. In this work we carried out the discrete range-only processor analyses numerically and the continuous intensity-only processors analyses using approximations derived from the Chernoff bounds[13,14].

Parameter interdependences

The processor equations contain many parameters: M, the number of subframes per frame; N, the number of pixels per subframe; Q, the number of range bins per pixel; CNR_t, the target CNR; CNR_b, the CNR of the background pixels; and the contrast ratio, $\zeta \equiv CNR_t/CNR_b$. Some of these parameters depend on each other through the radar equation,[6,17] so we cannot change them without accounting for the effect on other parameters (most notably, the CNRs). It is important to understand these relationships because we want to compare radars with different resolution capabilities imaging the same target and background environment. If we do not account for these parameter interdependences, the comparisons are not valid.

For simplicity, we examine the radar equation with α, the atmospheric extinction, = 0, and optical efficiency, $\varepsilon = 1$, so the radar equation reduces to[13,17]:

$$CNR_i = \left(\frac{\eta \rho_i}{h\nu_o \pi}\right) \frac{P_T}{B} \frac{A_R}{L_i^2} \qquad (i = t \text{ or } b) \qquad (14)$$

where η is the detector quantum efficiency, $h\nu_o$ is the optical photon energy, ρ_i is the speckle reflector diffuse reflectivity (which is constant), P_T is the transmitter peak power, B is the matched filter bandwidth, A_R is the radar optics area, and L_i is the reflector range. The subscript i can be either t, for the target, or b, for the background.

If we change A_R, the radar aperture area, we will change N, the number of pixels on the target. Both P_T, the radar peak transmitted power, and B, the radar bandwidth, are related to Q, the number of range bins per pixel, and also whether the laser itself is peak power limited or average power limited.

If we define a CNR at maximum radar aperture, $A_R^{(max)}$, and maximum bandwidth, $B^{(max)}$:

$$CNR_i^{(0)} = \left(\frac{\eta \rho_i}{h\nu_o}\right) \frac{A_R^{(max)}}{\pi L_i^2} \frac{P_T}{B^{(max)}} \qquad (i = t \text{ or } b) \qquad (15)$$

we can find equations for CNR_i at various N and Q values for peak (P_T) and average (P_{AV}) power limited lasers:

$$CNR_i = \begin{cases} CNR_i^{(0)} \dfrac{Q^{(max)}}{Q} \dfrac{N}{N^{(max)}} & : P_T \text{ limited} \\ CNR_i^{(0)} \dfrac{N}{N^{(max)}} & : P_{AV} \text{ limited} \end{cases} \qquad (i = t \text{ or } b) \qquad (16)$$

The value $Q^{(max)}$ exists because if Q gets too large, we would violate the assumption of a range unresolved target. The value $N^{(max)}$ simply represents the maximum aperture size, $A_R^{(max)}$, for any given system design.

In all the calculations that follow, we set $N^{(max)}$ = 40 pixels, $Q^{(max)}$ = 10,000 bins, and M = 1000. (Changing radar parameters does not affect M.)

Intensity-only processor

First we will examine the intensity-only processor, Equation (10), dependence on target CNR then look at the dependence on Q and N. In each case we plot P_M as a function of the one variable of interest and keep all the others constant. Figure 6 plots P_M versus CNR_t for N = 10 (part a) and N = 20 (part b). In each case a plot is shown for contrast ratios of ζ = +5 dB and +10 dB and for two P_F values, $P_F = 10^{-3}$ and $P_F = 10^{-6}$. M and Q are constant at M = 1000 and Q = 10.

There are two important aspects to these plots which bear explaining. First, as CNR_t gets large, the P_M approaches a non-zero asymptote. This occurs because we approach the speckle limited performance regime. At high CNR_t values there is essentially no LO shot noise to contend with and performance is limited by the speckle induced fluctuations in target and background intensities. Second, for large positive contrasts, the performance improves. For negative contrasts, even large ones, the performance is very poor. For the no contrast case it is easy to understand why the processor can do no better than to guess: it is looking for contrast and there is none. The poorer performance at large negative contrasts than at large positive contrasts is a result of the asymmetry of the density functions for the intensities under the two hypotheses. For negative contrasts, the target mean intensity is lower than the background mean intensity. However, the speckle induced fluctuations in the background measurements often give intensities less than the background mean and closer to the target mean intensity. This makes the two virtually impossible to distinguish at realistically low P_F values.

Figure 7a shown P_M as a function of Q, the number of range bins, for a constant average power laser while Figure 7b shows the same information for a constant peak power laser. In each case plots are for two values of N, 10 and 20 pixels, and two values of $CNR_t^{(0)}$, 16 and 20 dB, with fixed values of M = 1000, $P_F = 10^{-6}$, and ζ = +10 dB. The figures incorporate the CNR corrections for changing N and Q values.

For the constant peak laser power model, the performance falls at high Q values since the CNR depends on Q. As Q increases, the CNR drops until it moves away from the speckle limited performance regime. The weak Q dependence in the constant average laser power

model performance is due to the weak dependence of anomaly probability P_A, on Q shown in Equation (3). As Q increases, the probability of anomaly also increases slowly which causes a drop in performance.

Figure 8a plots P_M versus N, the number of pixels per subframe, for a constant average power laser, while Figure 8b plots the same quantities for a constant peak power laser. The plots are for $CNR_t(0)$ values of 16 and 20 dB and Q values of 10 and 1000 bins. Again, $P_F = 10^{-6}$ and M = 1000 subframes. The plots account for the CNR variations with N and Q. From the form of the Chernoff bounds,[13,14] we expect the performance to improve exponentially for increasing N values and the figures bear this out. The differences in the two plots are due to the differences in performance for changing Q values between the two laser models. These effects we have just discussed above.

Range-only processor

Now we examine the range-only processor of Equation (12). We will examine the same variables we did for the intensity-only processor. Figure 9 plots P_M versus CNR_t for N = 10 (part a) and N = 20 (part b). Three contrast ratios are shown and two P_F values, while Q = 10 and M = 1000 are constant. Here the performance improves as CNR_t gets larger and does not bottom out at a non-zero asymptotic value. As CNR_t gets larger, P_A goes to zero and there are no anomalies to confuse the processor, so it can perform arbitrarily well. We also notice for a fixed CNR_t, performance gets poorer as contrast increases. This occurs because as ζ increases for a fixed CNR_t, CNR_b must decrease. As CNR_b decreases, the processor has more difficulty distinguishing the background and performance falls off.

Figure 10 plots P_M versus Q for constant average laser power (part a) and constant peak laser power (part b). For the constant average power laser, the performance increases as Q increases for a while then starts to fall slowly. This is a result of two competing factors. As Q increases, the probability of getting anomalies (which occur in random bins) to clump together well enough to masquerade as a target falls. This improves performance. However, as Q increases, P_A also increases approximately logarithmically as shown in Equation (3). This causes performance to fall. For the constant peak power laser, the increase in CNR_t as Q falls overwhelms the weaker Q dependence in P_A. Performance improves quickly as Q decreases.

Performance comparisons

There are many ways to present the performance data and the number of variables we have available makes it difficult to present more than a small portion of the data at one time. Figure 11 shows a way to present the data that could be particularly useful to a system engineer. In this plot we select specified values for P_F and P_M at a certain CNR_t and ζ. Then we check to see if the range-only or intensity-only processor meets the performance criteria for various N and Q values. These plots then indicate the minimum combinations of angular and range resolutions required to meet the performance specifications.

Figure 11, for the constant average laser power model, shows the more significant impact of laser aperture size, A_R, (reflected in the N value) on performance relative to the range resolution parameter Q. Generally the processor either meets requirements for a given N or not, regardless of Q. Figure 11a is for relatively high performance requirements: P_D = 99.9% at $P_F = 10^{-6}$ and fairly low $CNR_t(0)$ values. At 16 dB, we find the point N = 20 pixels, Q = 10 bins where the intensity-only processor out-performs the range-only processor. At higher Q values, $\geq$ 300, the intensity-only processor fails, but the range-only processor satisfies the requirements for Q $\geq$ 30. If we increase the $CNR_t(0)$ by only 4 dB, we can meet requirements with either processor as long as N $\geq$ 20.

In Figure 11b we relax the performance requirements somewhat to PD = 95% at PF = 10-3, but we reduce the contrast to only 5 dB. Here the intensity-only processors need at least N = 30 pixels to meet the relaxed requirements because they perform so poorly at low contrasts. The range-only processors perform well enough, however, that for a 4 dB increase in $CNR_t(0)$, we can cut angular resolution in half, from N = 20 pixels to N = 10, pixels and still meet requirements.

Figure 12 is a presentation identical to Figure 11, but now for a laser of constant peak power. Here the processors both perform better at low Q values and poorer at high Q values because the CNR rises for smaller Q values, as shown in Equation (16). Now it is possible for the range-only processor to meet the performance criteria at lower angular resolution (N values) than before because of the increased CNR at low Q values.

Conclusions

In this paper we have seen how it is possible to derive nearly optimal processors for the binary hypothesis testing problem and use the statistics to find the performance of the

processors. We found the quasi-optimal processors are much like those researchers have used on an ad hoc basis. Although this paper presented only the ranging radar results, exact dualities exist[13] which apply the results directly to radars measuring intensity, range, Doppler, or any combination of these three. The processors were derived from realistic models assuming numerous unknown parameters: target range, target angular position, target reflectivity, and background reflectivity. Since it is possible to predict the performance of these processors analytically, we were able to show how performance varies as a function of target size, angular resolution or radar aperture, range resolution, target-to-background contrast, and overall CNR. A few case studies were presented as examples. These results make it possible for a system engineer to select appropriate design criteria for a laser radar and predict how changes in one parameter interact with other parameters. They are also useful because they demonstrate the limits to system performance dictated by the noise and speckle statistics. These results are useful as benchmarks against which other processors, even ad hoc ones, can be measured.

Acknowledgements

This research was supported in part by U. S. Army Research Office Contract DAAG29-84-K-0095. The numerical analyses were carried out at MIT Lincoln Laboratory.

References

1. Bachman, C. G., Laser Radar Systems and Techniques, Artech House, Dedham, MA, 1979.

2. Harney, R. C., Conceptual Design of a Multifunction Infrared Radar for the Tactical Aircraft Ground Attack Scenario, MIT Lincoln Lab, Project Report TST-25, 25 August 1978.

3. Del Boca, R. L. and Mongeon, R. J., "Multifunction CO_2 Laser Radar Technology," Proceedings SPIE, Vol. 300, pp 19-32, 1981.

4. Biron, D. G. and Edwards, B. E., "Moving Target Imaging Radar Utilizing both Intensity and Velocity Information," Technical Digest of Conference on Lasers and Electro-Optics, paper TB-6, Optical Society of America, Phoenix, AZ, 1982.

5. Gschwendtner, A. B., Harney, R. C., and Hull, R. J., "Coherent IR Radar Technology," Optical and Laser Remote Sensing, D. K. Killinger and A. Mooradian (eds), Springer-Verlag, Berlin, 1983.

6. Shapiro, J. H., Capron, B. A., and Harney, R. C., "Imaging and Target Detection with a Heterodyne-Reception Optical Radar," Applied Optics, Vol. 20, pp 3292-3313, 1981.

7. Wang, J. Y., Bartholomew, B. J., Streiff, M. C., and Starr, E. F., "Imaging CO_2 Laser Radar Field Tests," Applied Optics, Vol. 23, pp 2526-2571, 1984.

8. Letalick, D., Renhorn, I., and Steinvall, O., "Measured Signal Amplitude Distributions for a Coherent FM-CW CO_2 Laser Radar," Applied Optics Vol. 25, pp 3927-3938, 1986.

9. Letalick, D., Renhorn, I., and Steinvall, O., "Target and Atmospheric Influence on Coherent CO_2 Laser Radar Performance," Applied Optics, Vol. 25, pp 3939-3945, 1986.

10. Sullivan, D. R., "Active 10.6 μm Image Processing," Proceedings SPIE, Vol. 238, pp 103-116, 1980.

11. Lee, C. C., "Modified Distance Transform and Linking Algorithm for Image Skeletonization," Proceedings SPIE, Vol 415, pp 147-154, 1983.

12. Shapiro, J. H., Reinhold, R. W., and Park, D., "Performance Analyses for Peak-Detecting Laser Radars," Proceedings SPIE, Vol. 663, pp 38-58, 1986.

13. Mark, M. B., "Multipixel, Multidimensional Laser Radar System Performance," PhD Thesis, Dept of Electrical Engineering and Computer Science, MIT, 1986.

14. Van Trees, H. L., Detection, Estimation, and Modulation Theory, Part I, John Wiley and Sons, New York, 1986.

15. Harney, R. C., and Hull, R. J., "Compact Infrared Radar Technology," Proceedings SPIE, Vol. 227, pp 162-170, 1980.

16. Hannon, S. M., "Performance Analysis of Quasi-Optimal, Multipixel Laser Radar System Processors," SM Thesis, Dept of Electrical Engineering and Computer Science, MIT, 1987.

17. Shapiro, J. H., "Target Reflectivity Theory for Coherent Laser Radars," Applied Optics, Vol. 21, pp 3398-3407, 1982.

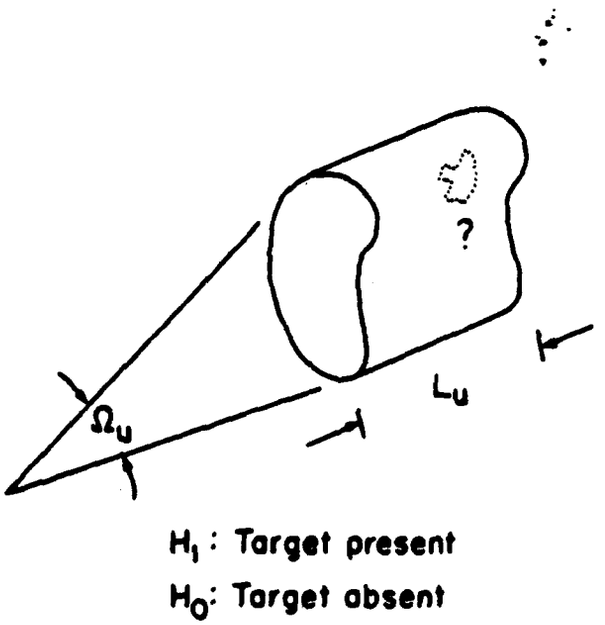

Figure 1. The target detection problem.

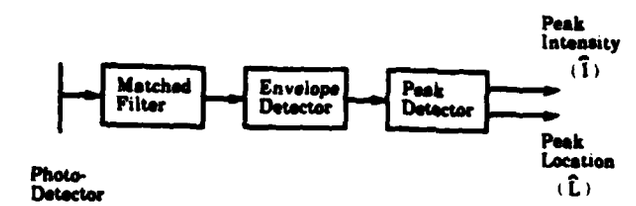

Figure 2. Pre-processor structure for a ranging radar.

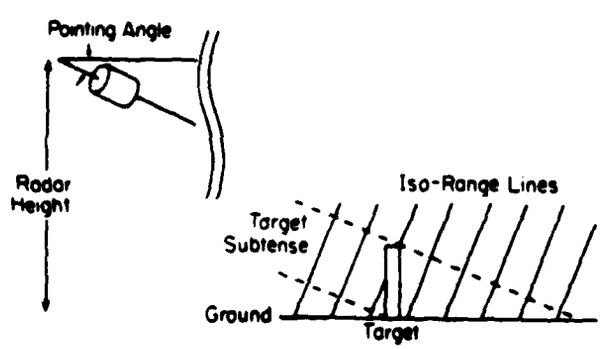

Figure 3. Laser-target geometry model.

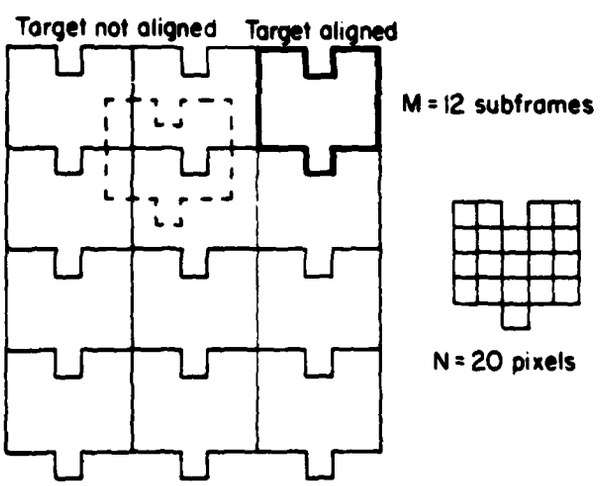

Figure 4. Target subframe model.

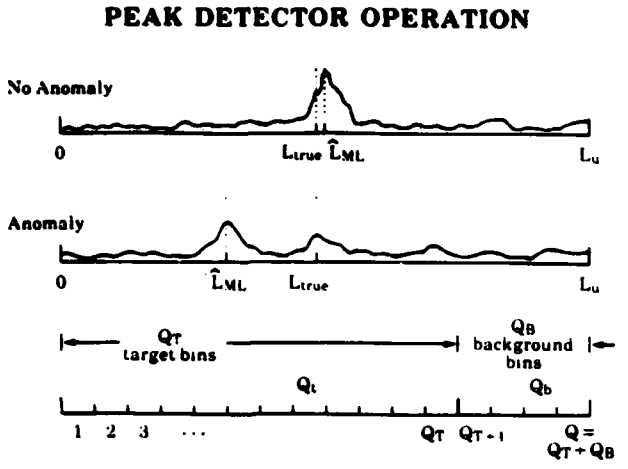

Figure 5. Range-bin model for peak detection.

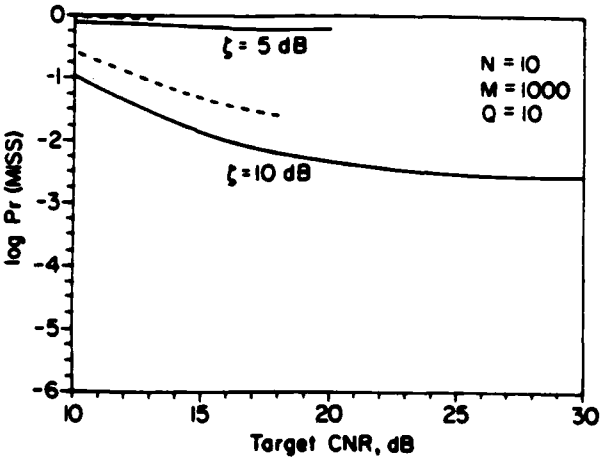

Figure 6 (a). Intensity-only processor miss probability, P_M, vs. target carrier-to-noise ratio, CNR_c, for N=10 pixels per subframe, M=1000 subframes per frame, and Q=10 range bins. Upper two curves are for ζ=5 dB target contrast; lower two curves are for ζ=10 dB target contrast. Dashed curves are for false-alarm probability $P_F=10^{-6}$; solid curves are for $P_F=10^{-3}$.

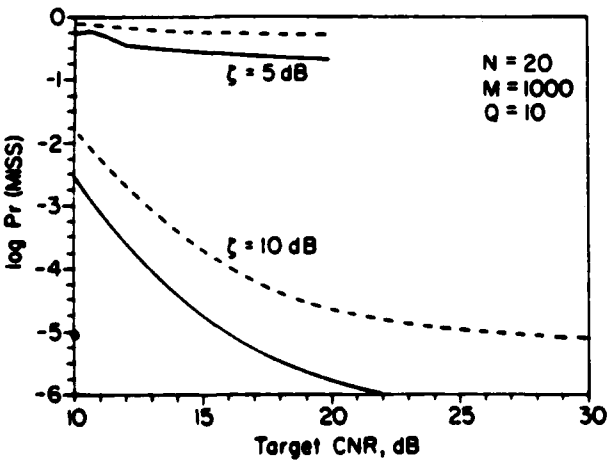

Figure 6 (b). Intensity-only processor miss probability, P_M, vs. target carrier-to-noise ratio, CNR_c, for N=20 pixels per subframe, M=1000 subframes per frame, and Q=10 range bins. Upper two curves are for ζ=5 dB target contrast; lower two curves are for ζ=10 dB target contrast. Dashed curves are for false-alarm probability $P_F=10^{-6}$; solid curves are for $P_F=10^{-3}$.

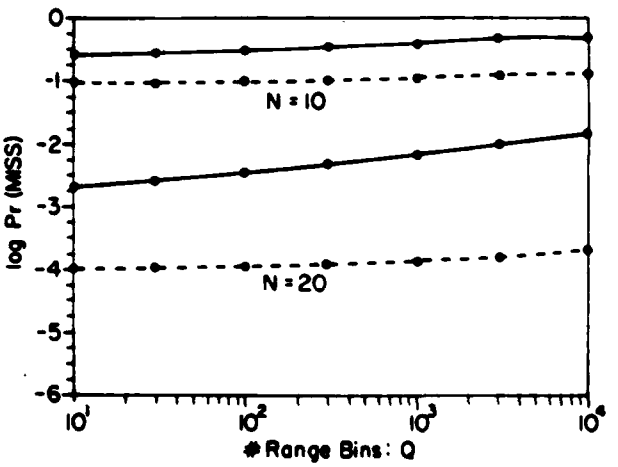

Figure 7 (a). Intensity-only processor miss probability, P_M, vs. number of range bins, Q, for constant-P_{AV} laser model with M=1000 subframes per frame, $P_F=10^{-6}$ false-alarm probability, and ζ=10 dB target contrast. Upper two curves are for N=10 pixels per subframe; lower curves are for N=20 pixels per subframe. Dashed curves are for $CNR_c^{(0)}$=20 dB; solid curves are for $CNR_c^{(0)}$=16 dB.

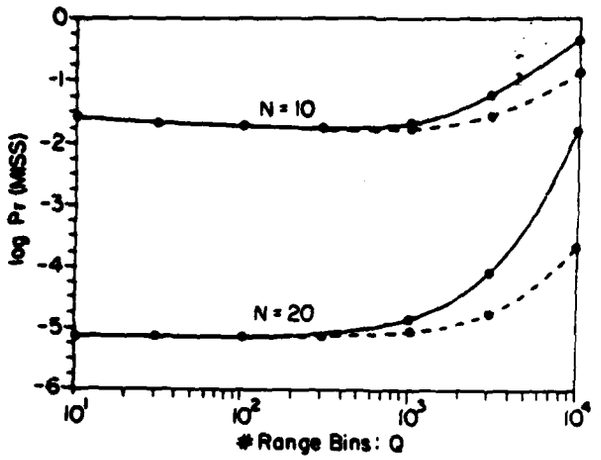

Figure 7 (b). Intensity-only processor miss probability, P_M, vs. number of range bins, Q, for constant-P_T laser model with M=1000 subframes per frame, $P_F=10^{-6}$ false-alarm probability, and ζ=10 dB target contrast. Upper two curves are for N=10 pixels per subframe; lower two curves are for N=20 pixels per subframe. Dashed curves are for $CNR_t^{(Q)}$=20 dB; solid curves are for $CNR_t^{(Q)}$=16 dB.

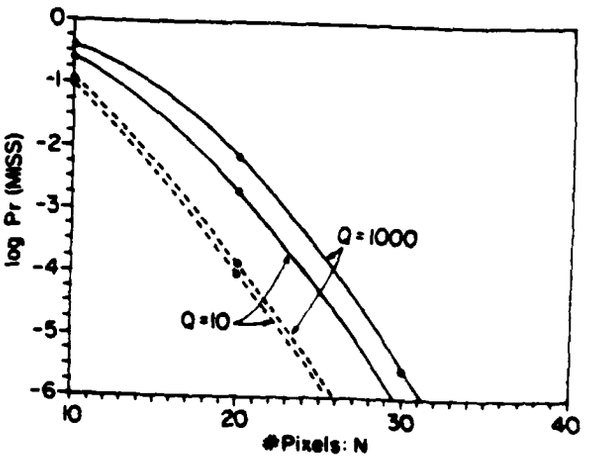

Figure 8 (a). Intensity-only processor miss probability, P_M, vs. number of subframe pixels, N, for constant-P_{Av} laser model with M=1000 subframes per frame, $P_F=10^{-6}$ false-alarm probability, and ζ=10 dB target contrast. Arrows indicate curves for Q=10 and Q=1000 range bins. Dashed curves are for $CNR_t^{(Q)}$=20 dB; solid curves are for $CNR_t^{(Q)}$=16 dB.

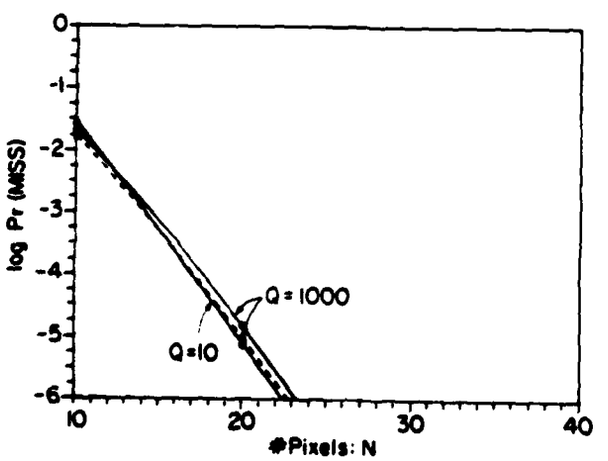

Figure 8 (b). Intensity-only processor miss probability, P_M, vs. number of subframe pixels, N, for constant-P_T laser model with M=1000 subframes per frame, $P_F=10^{-6}$ false-alarm probability, and ζ=10 dB target contrast. Arrows indicate curves for Q=10 and Q=1000 range bins. Dashed and solid Q=1000 curves are for $CNR_t^{(Q)}$=20 dB and $CNR_t^{(Q)}$=16 dB, respectively; Q=10 curve is for both $CNR_t^{(Q)}$=20 dB and $CNR_t^{(Q)}$=16 dB.

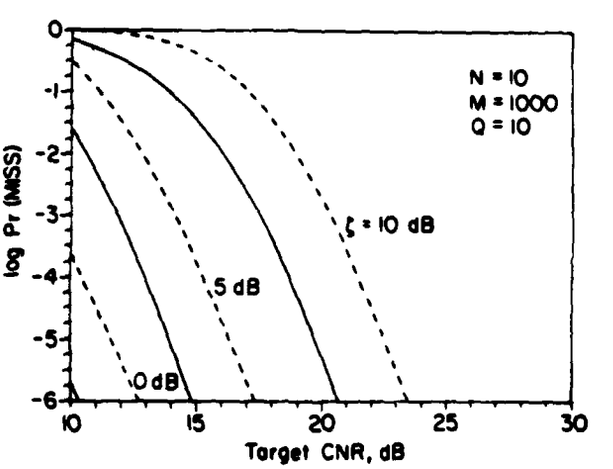

Figure 9 (a). Range-only processor miss probability, P_M, vs. target carrier-to-noise ratio, CNR_t, for N=10 pixels per subframe, M=1000 subframes per frame, and Q=10 range bins. Rightmost two curves are for ζ=10 dB target contrast; middle two curves are for ζ=5 dB target contrast; leftmost two curves are for ζ=0 dB target contrast. Dashed curves are for false-alarm probability $P_F=10^{-6}$; solid curves are for $P_F=10^{-3}$.

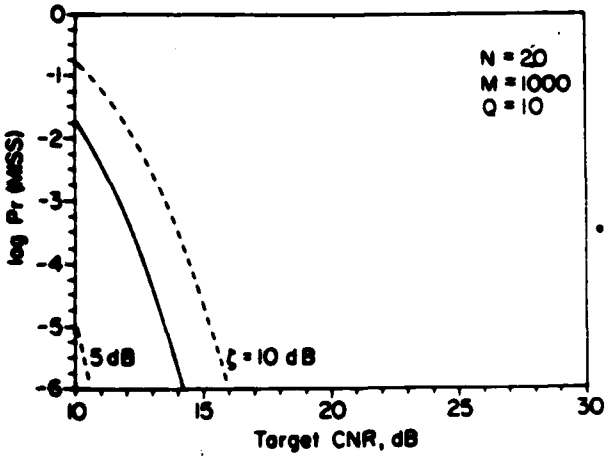

Figure 9 (b). Range-only processor miss probability, P_M, vs. target carrier-to-noise ratio, CNR_t, for N=20 pixels per subframe, M=1000 subframes per frame, and Q=10 range bins. Rightmost two curves are for ζ=10 dB target contrast; leftmost curve is for ζ=5 dB target contrast. Dashed curves are for false-alarm probability $P_F=10^{-6}$; solid curve is for $P_F=10^{-3}$.

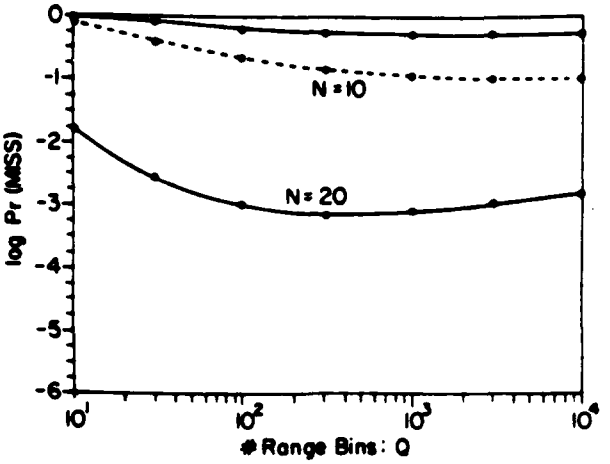

Figure 10(a). Range-only processor miss probability, P_M, vs. number of range bins, Q, for constant-P_{AV} laser model with M=1000 subframes per frame, $P_F=10^{-6}$ false-alarm probability, and ζ=10 dB target contrast. Upper two curves are for N=10 pixels per subframe; bottom curve is for N=20 pixels per subframe. Dashed curve is for $CNR_t^{(Q)}$=20 dB; solid curves are for $CNR_t^{(Q)}$=16 dB.

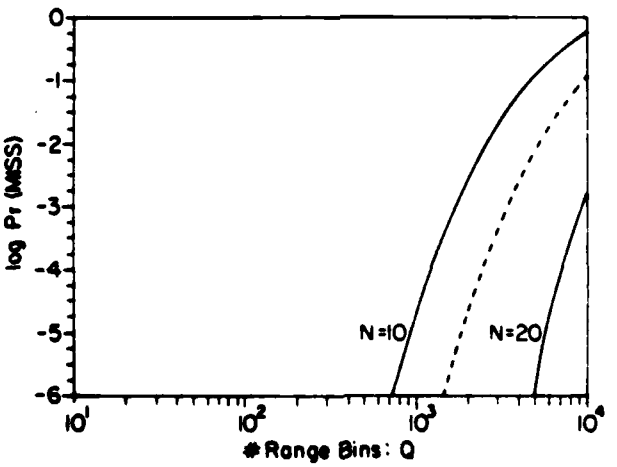

Figure 10 (b). Range-only processor miss probability, P_M, vs. number of range bins, Q, for constant-P_T laser model with M=1000 subframes per frame, $P_F=10^{-6}$ false alarm probability, and ζ=10 dB target contrast. Leftmost two curves are for N=10 pixels per subframe; rightmost curve is for N=20 pixels per subframe. Dashed curve is for $CNR_t^{(Q)}$=20 dB; solid curves are for $CNR_t^{(Q)}$=16 dB.

N \ log(Q)	1.0	1.5	2.0	2.5	3.0	3.5	4.0
10							
20	RI	RI	RI	RI	RI	RI	RI
30	RI	RI	RI	RI	RI	RI	RI
40	RI	RI	RI	RI	RI	RI	RI

$CNR_t^{(0)} = 20$ dB

N \ log(Q)	1.0	1.5	2.0	2.5	3.0	3.5	4.0
10							
20	I	RI	RI	R	R	R	R
30	RI	RI	RI	RI	RI	RI	RI
40	RI	RI	RI	RI	RI	RI	RI

$CNR_t^{(0)} = 16$ dB

Figure 11. (a) Target-detection performance trade-offs for constant-P_{AV} laser model with M=1000 subframes. High-performance/high-contrast case: "R" = range-only processor achieves $P_M \leq 10^{-3}$ at $P_F = 10^{-6}$ for $\zeta = 10$ dB target contrast; "I" = intensity-only processor achieves $P_M \leq 10^{-3}$ at $P_F = 10^{-6}$ for $\zeta = 10$ dB target contrast.

N \ log(Q)	1.0	1.5	2.0	2.5	3.0	3.5	4.0
10	R	R	R	R	R	R	R
20	R	R	R	R	R	R	R
30	RI	RI	RI	RI	RI	RI	RI
40	RI	RI	RI	RI	RI	RI	RI

$CNR_t^{(0)} = 20$ dB

N \ log(Q)	1.0	1.5	2.0	2.5	3.0	3.5	4.0
10							
20	R	R	R	R	R	R	R
30	RI	RI	RI	RI	RI	RI	RI
40	RI	RI	RI	RI	RI	RI	RI

$CNR_t^{(0)} = 16$ dB

Figure 11. (b) Target-detection performance trade-offs for constant-P_{AV} laser model with M=1000 subframes. Low-performance/low-contrast case: "R" = range-only processor achieves $P_M \leq 0.05$ at $P_F = 10^{-3}$ for $\zeta = 5$ dB target contrast; "I" = intensity-only processor achieves $P_M \leq 0.05$ at $P_F = 10^{-3}$ for $\zeta = 5$ dB target contrast.

N \ log(Q)	1.0	1.5	2.0	2.5	3.0	3.5	4.0
10	R	R	R	R	R	R	
20	RI	RI	RI	RI	RI	RI	RI
30	RI	RI	RI	RI	RI	RI	RI
40	RI	RI	RI	RI	RI	RI	RI

$CNR_t^{(0)} = 20$ dB

N \ log(Q)	1.0	1.5	2.0	2.5	3.0	3.5	4.0
10	R	R	R	R	R		
20	RI	RI	RI	RI	RI	RI	R
30	RI	RI	RI	RI	RI	RI	RI
40	RI	RI	RI	RI	RI	RI	RI

$CNR_t^{(0)} = 16$ dB

Figure 12. (a) Target-detection performance tradeoffs for constant-P_T laser model with M = 1000 subframes. High-performance/high-contrast case: "R" = range-only processor achieves $P_M \leq 10^{-3}$ at $P_F = 10^{-6}$ for $\zeta = 10$ dB target contrast; "I" = intensity-only processor achieves $P_M \leq 10^{-3}$ at $P_F = 10^{-6}$ for $\zeta = 10$ dB target contrast.

N \ log(Q)	1.0	1.5	2.0	2.5	3.0	3.5	4.0
10	R	R	R	R	R	R	R
20	R	R	R	R	R	R	R
30	RI	RI	RI	RI	RI	RI	RI
40	RI	RI	RI	RI	RI	RI	RI

$CNR_t^{(0)} = 20$ dB

N \ log(Q)	1.0	1.5	2.0	2.5	3.0	3.5	4.0
10	R	R	R	R	R	R	
20	R	R	R	R	R	R	R
30	RI	RI	RI	RI	RI	RI	RI
40	RI	RI	RI	RI	RI	RI	RI

$CNR_t^{(0)} = 16$ dB

Figure 12. (b) Target-detection performance trade-offs for constant-P_T laser model with M = 1000 subframes. Low-performance/low-contrast case: "R" = range-only processor achieves $P_M \leq 0.05$ at $P_F = 10^{-3}$ for $\zeta = 5$ dB target contrast; "I" = intensity-only processor achieves $P_M \leq 0.05$ at $P_F = 10^{-3}$ for $\zeta = 5$ dB target contrast.

END

FILMED

MARCH, 1988

DTIC